New Phytologist

The *Medicago truncatula* nodule-specific cysteine-rich peptides, NCR343 and NCR-new35 are required for the maintenance of rhizobia in nitrogen-fixing nodules

Beatrix Horváth[1]*, Berivan Güngör[1,2]*, Mónika Tóth[1], Ágota Domonkos[1], Ferhan Ayaydin[3,4], Farheen Saifi[1], Yuhui Chen[5], János Barnabás Biró[1,2], Mickael Bourge[6], Zoltán Szabó[1], Zoltán Tóth[1], Rujin Chen[5] and Péter Kaló[1,2]

[1]Institute of Genetics and Biotechnology, Hungarian University of Agriculture and Life Sciences, Gödöllő, 2100, Hungary; [2]Institute of Plant Biology, Biological Research Centre, Eötvös Lóránd Research Network, Szeged, 6726, Hungary; [3]Hungarian Centre of Excellence for Molecular Medicine (HCEMM) Nonprofit Ltd, Szeged, 6728, Hungary; [4]Cellular Imaging Laboratory, Biological Research Centre, Eötvös Lóránd Research Network, Szeged, 6726, Hungary; [5]School of Life Sciences, Lanzhou University, Lanzhou, 730000, China; [6]Cytometry Facility, Imagerie-Gif, Université Paris-Saclay, CEA, CNRS, Institute for Integrative Biology of the Cell (I2BC), Gif-sur-Yvette, 91198, France

Author for correspondence:
Péter Kaló
Email: *kalo.peter@brc.hu*

Received: *19 February 2023*
Accepted: *18 May 2023*

New Phytologist (2023) **239:** 1974–1988
doi: 10.1111/nph.19097

Key words: indeterminate nodule, legume, *Medicago truncatula*, nitrogen-fixing symbiosis, nodule-specific cysteine-rich peptide.

Summary

- In the nodules of IRLC legumes, including *Medicago truncatula*, nitrogen-fixing rhizobia undergo terminal differentiation resulting in elongated and endoreduplicated bacteroids specialized for nitrogen fixation. This irreversible transition of rhizobia is mediated by host produced nodule-specific cysteine-rich (NCR) peptides, of which *c*. 700 are encoded in the *M*. *truncatula* genome but only few of them have been proved to be essential for nitrogen fixation.
- We carried out the characterization of the nodulation phenotype of three ineffective nitrogen-fixing *M*. *truncatula* mutants using confocal and electron microscopy, monitored the expression of defence and senescence-related marker genes, and analysed the bacteroid differentiation with flow cytometry. Genetic mapping combined with microarray- or transcriptome-based cloning was used to identify the impaired genes.
- *Mtsym19* and *Mtsym20* mutants are defective in the same peptide NCR-new35 and the lack of *NCR343* is responsible for the ineffective symbiosis of NF-FN9363. We found that the expression of *NCR-new35* is significantly lower and limited to the transition zone of the nodule compared with other crucial *NCRs*. The fluorescent protein-tagged version of NCR343 and NCR-new35 localized to the symbiotic compartment.
- Our discovery added two additional members to the group of *NCR* genes essential for nitrogen-fixing symbiosis in *M*. *truncatula*.

Introduction

Legumes can establish nitrogen-fixing endosymbiotic association with soil bacteria, collectively termed rhizobia. This interaction results in the formation of nodules, generally formed on the roots, where rhizobia are hosted and convert atmospheric dinitrogen to ammonia. The mutual recognition and fine-tuned communication between the host legume and rhizobia lead to two synchronous developmental processes, rhizobial infection and initiation of nodule primordia by activating the mitosis of certain root cortical cells (Oldroyd & Downie, 2008). Rhizobial colonization occurs either through infection threads (ITs) formed in root hair cells or through intercellular transition. Within infected nodule cells, bacteria are encompassed by a plant-derived membrane resulting in the formation of subcellular compartments called symbiosomes. Bacteria multiply and undergo morphological and metabolic transition to adapt from free-living lifestyle to their advanced endosymbiotic form termed bacteroids (Jones *et al*., 2007).

Nodules formed on legume roots are classified into two types: indeterminate or determinate, based on the term of their meristem activity (Hirsch, 1992). The cylindrical shaped indeterminate nodules, such as those found on *Medicago truncatula* roots, possess a persistent meristem during the lifespan of the nodules, and as a result, the mature indeterminate nodules consist of a developmental gradient of cells forming distinct zones (Vasse *et al*., 1990). The mitotic activity of meristem cells (zone I, ZI), located at the nodule apex, produces new cells for all nodule tissues. Cells leaving the meristem are relatively small with a large central vacuole (Gavrin *et al*., 2014) and have a fourfold haploid

*These authors contributed equally to this work.

DNA content (4C; Nagymihaly *et al.*, 2017). In these cells in the distal part of the infection zone (ZIId), rod-shaped rhizobia are released from ITs to the host cell cytoplasm and from hereafter, both rhizobia and infected nodule cells undergo differentiation processes through the subsequent nodule zones. The transition of symbiotic cells and rhizobia involves the replication of their genomes without cytokinesis resulting in enlargement of invaded host cells and elongation of bacteria (Vasse *et al.*, 1990; Mergaert *et al.*, 2006; Nagymihaly *et al.*, 2017). The enlarged symbiotic cells in the proximal part of the infection zone (ZIIp) have a DNA content of 8C/16C and their volume is almost entirely occupied by distended vacuoles. In cells of the first few layers of the nitrogen fixation zone (ZIIId, also termed as transition zone or interzone between ZII and ZIII and referred hereafter IZ in this study), elongated bacteroids surround the collapsed central vacuoles of infected host cells (16C/32C) which are filled with starch granules. Rhizobia and host cells complete their differentiation in IZ and nitrogen fixation begins in massive symbiotic cells having highly endoreduplicated chromosomes (32C/64C) and large volume vacuoles (nitrogen fixation zone, ZIII). As indeterminate nodule ages, proximal to the root, a senescence zone (ZIV) evolves wherein the symbiotic interaction terminates and both infected host cells and rhizobia degrade.

Rhizobia, hosted in the nodules of legumes of the Inverted Repeat-Lacking Clade (IRLC) such as the genera of *Medicago*, *Pisum*, *Trifolium*, *Vicia*, etc., and *Aeschynomene* species undergo terminal differentiation (Mergaert *et al.*, 2006; Czernic *et al.*, 2015). These differentiated bacteroids, reaching 5–10 µm in length and DNA content of 24C in fully differentiated form in *M. truncatula* nodules, are not able to regrow and proliferate outside the indeterminate nodules. This irreversible transition of rhizobia in *M. truncatula* nodules is mediated by host-produced nodule-specific cysteine-rich (NCR) peptides (Van de Velde *et al.*, 2010). The genome of *M. truncatula* encodes for *c.* 700 NCR peptides and similar genes in different numbers have been identified in other IRLC legumes (Mergaert *et al.*, 2003; Montiel *et al.*, 2017; Wei *et al.*, 2022; Zorin *et al.*, 2022). Almost all *NCR* genes are specifically expressed in infected cells of *M. truncatula* nodules, and they are activated in successive waves during nodule organogenesis and bacteroid differentiation (Nallu *et al.*, 2013; Guefrachi *et al.*, 2014). NCR peptides possess highly conserved N-terminal signals which are recognized by the secretion complex of the nodule cells (Wang *et al.*, 2010). The secretory pathway delivers the mature NCR peptides, usually 35–55 residues in length, to the symbiosomes inducing bacteroid differentiation. The characteristic feature of NCR peptides is the four or six cysteine residues in conserved positions which are presumed to be involved in the formation of intra- and intermolecular disulphide bonds (Mergaert *et al.*, 2003). The structural analysis of peptides NCR044 and NCR169 confirmed the presence of different pattern of disulphide bonds that contribute to the structural stability of the peptides (Velivelli *et al.*, 2020; Isozumi *et al.*, 2021). *Medicago truncatula* Thioredoxin s1, which reduces disulphide bonds, is also targeted to symbiosomes and suggested regulating the activity of NCR peptides by their redox state (Ribeiro *et al.*, 2017). These results implied the importance of cysteine residues but ultimately, the substitution of the conserved cysteine for serine evidenced the requirement of cysteines for the symbiotic function of peptide NCR169 (Horvath *et al.*, 2015).

The high number of *NCR* genes in the *M. truncatula* genome implied that they act redundantly. Forward genetic studies of deletion mutants deficient in single NCR peptides, NCR169 or NCR211, revealed that these peptides are essential for bacteroid differentiation and persistence in *M. truncatula* nodules (Horvath *et al.*, 2015; Kim *et al.*, 2015). Despite these findings, little knowledge is available about the molecular mechanism of NCR peptides mediating bacteroid differentiation *in planta*. A recent reverse genetic analysis of *NCR247* demonstrated that NCR247 is required for nodule functioning and provided experimental data about the operation of one of the NCR peptides (Sankari *et al.*, 2022). In addition to the prominent positive regulatory role of these NCR peptides in the symbiotic interaction, other NCR peptides, NFS1 and NFS2, control bacterial survival in a strain- and allele-specific manner and negatively regulate the nitrogen-fixing symbiosis in *M. truncatula* (Wang *et al.*, 2017; Yang *et al.*, 2017).

In this report, we present the phenotypic analysis of three *M. truncatula* symbiotic nitrogen-fixing mutants *Mtsym19*, *Mtsym20* and NF-FN9363. In these ineffective symbiotic nodules, the bacteroid differentiation was incomplete suggesting the function of the impaired genes in this developmental step. We found that *Mtsym19* and *Mtsym20* are defective in the same gene, *NCR-new35* and the deletion of *NCR343* in mutant NF-FN9363 resulted in the ineffective symbiotic phenotype. We show that the substitution of the first cysteine residue either in NCR-new35 or NCR343 abolishes the symbiotic function of these peptides. Our results indicate that the peptides NCR-new35 and NCR343 are essential for terminal bacteroid differentiation in *M. truncatula* nodules.

Materials and Methods

Plant materials, rhizobia strains and growth conditions

Symbiotic mutant NF-FN9363 was identified during a symbiotic screen of fast neutron bombarded *M. truncatula* A17 plants (Xi *et al.*, 2013). Mutants *M. truncatula sym18* (*Mtsym18*, TR36), *Mtsym19* (TR183) and *Mtsym20* (TRV43) were obtained following gamma ray irradiation of *M. truncatula* cv Jemalong seeds (Sagan *et al.*, 1995; Morandi *et al.*, 2005). *Medicago truncatula* Gaertn. cv Jemalong or genotype A17 were used as wild-type (WT) controls for characterization of the symbiotic phenotype of *Mtsym19*, *Mtsym20* and FN-NF9363. Four-day-old pre-grown plants were inoculated with the rhizobium strains *Sinorhizobium* (*Ensifer*) *medicae* WSM419, ABS7 or *S. meliloti* 1021 carrying the pXLGD4 plasmid expressing the *hemA::lacZ* reporter gene or strain *S. meliloti* FSM-MA carrying the pMEpTrpGUSGFP plasmid expressing the β-glucuronidase-GFP fusion protein. The condition of plant growth and inoculation with rhizobia were the same as described earlier (Domonkos *et al.*, 2017).

Histological analyses and microscopy

The nodulation phenotype of the ineffective mutant and WT plants was analysed at 3 wk post-inoculation (wpi) with different bacterial strains using a Leica MZ10-F stereo microscope (Leica Microsystems GmbH, Wetzlar, Germany). To assess bacterial colonization and analyse nodule cell structure and bacteroid morphology, mutant and WT plants were inoculated with rhizobia strains carrying the pXLGD4 plasmid. Nodule sections were stained for β-galactosidase activity or with SYTO13 (Thermo Fisher Scientific, Waltham, MA, USA) using the procedure described previously (Boivin *et al.*, 1990; Horvath *et al.*, 2015; Domonkos *et al.*, 2017). The promoter activity of the *NCR* genes was assayed with promoter-*GUS* reporter gene constructs generated using the Gateway cloning technology (Thermo Fisher Scientific). The assembly of the constructs and the method of GUS reporter assay are described in Supporting Information Methods S1.

Identification of deletions in the genome of *M. truncatula* symbiotic mutants

The database of copy number variations identified with whole genome array-based comparative genomic hybridization analysis of *M. truncatula* fast neutron bombarded mutant lines (https://medicago-mutant.dasnr.okstate.edu/mutant/index.php) was searched to identify mutagenesis events co-segregating with the symbiotic mutant locus of FN-NF9363. To detect genetic alterations in the genome of *Mtsym18*, *Mtsym19* and *Mtsym20*, an analysis of RNAseq data was carried out. Nodules of the symbiotic mutants were harvested at 2 wpi with *S. medicae* WSM419 in liquid nitrogen, total RNA was extracted with TRI Reagent (Sigma) and purified with Direct-zol RNA MiniPrep Kit (Zymo Research, Irvine, CA, USA). RNA samples were treated with DNaseI on Zymo-Spin columns according to the manufacturer's instructions to remove the genomic DNA. For the details of RNAseq, see Methods S1.

Gene expression analysis

The transcriptional activity of *NCR-new35*, *NCR211*, *NCR343*, *NCR169* as well as senescence- and defence-related genes was analysed with reverse transcription quantitative polymerase chain reaction (RT-qPCR). For the expression analysis of senescence- and defence-related genes, WT and mutant nodules of *nad1-3*, NF-FN9363, *Mtsym20*, *Mtdnf4-1* and *Mtdnf7-1* were harvested at 3 wpi with *S. medicae* WSM419. The transcription activity of *NCR* genes was monitored in WT nodules at 2 and 3 wpi. RNA was extracted in the same way as for RNAseq. Complementary DNA was prepared and RT-qPCR was carried out as formerly described (Kovacs *et al.*, 2021). Relative expression of the target genes was normalized using the housekeeping gene *Polypyrimidine tract-binding protein 2* (*PTB*, MtrunA17_Chr3g0126461) and a gene (MtrunA17_Chr3g0126781) with a ubiquitin domain. Primer sequences used for RT-qPCR are listed in Table S1.

Complementation experiments using hairy-root transformation and subcellular localization of NCR peptides

Constructs for genetic complementation experiments and study of the localization of NCR343 and NCR-new35 peptides in symbiotic nodule cells were generated using either single-site or multisite Gateway Recombination Cloning Technology (Thermo Fisher Scientific). Fragments to generate constructs for complementation, subcellular localization and substituting cysteines residues were amplified with Phusion DNA Polymerase (Thermo Fisher Scientific) using the *M. truncatula* cv Jemalong genomic DNA as template. Amplified fragments covering the native promoters, the genomic fragment and the 3′UTR regions of the *NCR341*, *NCR343*, *NCR345* and *NCR-new35* genes were cloned into pKGW-RR binary destination vector for complementation experiments. The construct for *NCR344* was assembled into pKm43GW-rolD::EGFP from three entry clones pDONRP4-P1R, pDONR221 and pDONRP2R-P3. The substitutions of the first cysteines to serines were generated with overlap extension PCR technology using overlapping mutated primers and the entry clones of *NCR343*, *NCR-new35* and *NCR211* created for complementation experiments. Mutated fragments were recombined into the binary vector pKm43GW-rolD::EGFP. To study the subcellular localization of NCR343 and NCR-new35 peptides, constructs coding for mCherry tagged versions of the peptides were generated in pK7m34GW-rolD::EGFP destination vector using Multisite Gateway Technology by assembling the three entry clones of the native promoters, the coding sequences without STOP codon and the mCherry protein, respectively. The details of the constructs, the procedure for plant transformation and the details of laser-scanning confocal microscopy (Visitron spinning disk confocal system; Visitron systems GmBH, Puchleim, Germany) are provided as Methods S1.

Miscellaneous methods

To measure the length of rhizobia, bacteroids were purified from WT and mutant nodules at 16 d post-inoculation (dpi), stained with propidium iodide (PI). The bacteroid length was determined on images captured by confocal microscopy (Leica TCS SP8; Leica Microsystems GmbH) and using the ImageJ software. For the details of analysis of elongation and DNA content of rhizobia, see Methods S1. Nodule samples were treated, and sections were prepared for scanning electron microscopy (SEM) as described earlier (Domonkos *et al.*, 2017). Multiple alignments of NCR peptide sequences and the NCR sequence logos were created using the CLC Genomics Workbench 9.5.3 program with default settings. The phylogenetic analysis was conducted on the Phylogeny.fr online platform (http://www.phylogeny.fr/simple_phylogeny.cgi). The alignment of the sequences was performed with the Muscle program (v.3.8.31), the phylogenetic tree was constructed using the maximum likelihood method using the PhyML program (v.3.1/3.0 aLRT) and visualized by TreeDyn (v.198.3).

Results

The nitrogen fixation zone of nodules of *M. truncatula* deletion mutants are defective in colonization by rhizobia

The NF-FN9363, *Mtsym19* and *Mtsym20* ineffective symbiotic (Fix-) mutants were identified formerly in genetic screens for symbiotic nitrogen fixation mutant populations (Sagan *et al.*, 1995; Morandi *et al.*, 2005; Xi *et al.*, 2013). *Mtsym19* and *Mtsym20* were reported representing distinct symbiotic loci (Morandi *et al.*, 2005) but based on the results described later, we found that these mutants are allelic and therefore only one allele was used in some experiments. The NF-FN9363 and *Mtsym20* ineffective mutants were inoculated with different rhizobia strains during the mutant screens. To test the strain dependence of the symbiotic phenotype of these mutants, the nodulation and growth phenotype of WT and NF-FN9363, *Mtsym20*, *Mtdnf4-1* and *Mtdnf7-2* (Starker *et al.*, 2006; Domonkos *et al.*, 2013) mutant plants were analysed 3 wpi with *S. meliloti* strains 1021 and FSM-MA and *S. medicae* strains ABS7 and WSM419. Mutant plants showed the symptoms of nitrogen starvation (yellow leaves, reduced growth) with all the tested rhizobia strains, even with the highly compatible *S. medicae* WSM419 strain (Fig. 1a; Terpolilli *et al.*, 2008). Mutant plants developed roundish or slightly cylindrical white nodules, indicating the absence of leghaemoglobin, with each tested rhizobia strain (Figs 1b, S1a). Nitrogen deficiency of the ineffective symbiotic mutants induced the development of increased number of nodules and resulted in reduced dry weight of the aerial part of mutant plants compared with WT plants at 3 wpi with each rhizobia strain (Fig. S1b).

To analyse the colonization of symbiotic nodules, mutant and WT plants were inoculated with *S. medicae* WSM419 (pXLGD4), which constitutively expresses the *lacZ* gene. Longitudinal sections of nodules were stained for β-galactosidase activity 14 dpi and the presence of rhizobia was analysed by light microscopy. WT nodules showed the characteristic zonation of indeterminate nodules colonized with rhizobia at this time point (Fig. 1b lower panel). Despite the fact that mutant nodules were reduced in size compared with WT ones, the zones of indeterminate nodules could be already identified in mutant nodules. Rhizobia-infected nodule cells were observed in the infection zone and interzone of mutant nodules indicating that the impaired symbiotic genes are essential for the differentiation or the persistence of differentiated rhizobia in mutants NF-FN9363, *Mtsym19* and *Mtsym20* (Fig. 1b lower panel). The nodule colonization in the three mutants was similar to that in *M. truncatula dnf4* and *dnf7* mutants defective in NCR peptides NCR211 and NCR169, respectively (Horvath *et al.*, 2015; Kim *et al.*, 2015). Therefore, and for the reasons described later, the mutants NF-FN9363, *Mtsym19* and *Mtsym20* were analysed along with the symbiotic mutants *Mtdnf4-1* and *Mtdnf7-2*.

To analyse nodule colonization in more detail, mutant and WT nodule sections were stained with nucleic acid-binding dye SYTO13 at 14 dpi with *S. medicae* WSM419 and examined by laser-scanning confocal microscopy that enabled the visualization of stained bacteria and plant nuclei fluoresced in cyan, the autofluorescent cell wall and accumulated polyphenolic compounds (red channel) simultaneously (Fig. 2). Nodules of WT plants showed rhizobia-colonized cells in the infection zone, interzone and nitrogen fixation zone (Fig. 2a1–a8). The bacterial invasion of ZII and IZ of mutant and WT nodules was similar, albeit the interzone, where bacteria complete their differentiation into

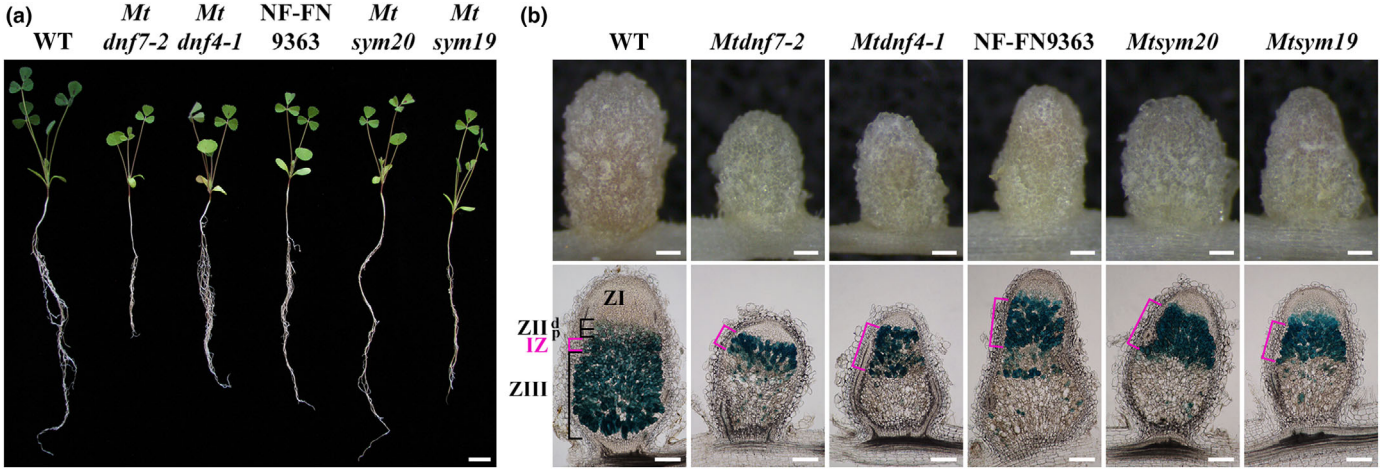

Fig. 1 The ineffective nodulation phenotype of *Medicago truncatula* symbiotic mutants *Mtdnf7-2*, *Mtdnf4-1*, NF-FN9363, *Mtsym20* and *Mtsym19*. (a) Ineffective nitrogen-fixing (Fix-) symbiotic mutants showed the symptoms of the nitrogen starvation (retarded growth, pale green leaves) compared with wild-type (WT) plant 2 wk following inoculation with strain *Sinorhizobium medicae* WSM419 carrying the *lacZ* reporter gene. (b) Slightly elongated white nodules were formed on the roots of the Fix- symbiotic mutant plants and cylindrical pink nodules were observed on WT roots 14 d post-inoculation (dpi) with *S. medicae* WSM419 (upper images). Longitudinal nodule sections stained for β-galactosidase activity show the normal colonization of nodule zones characteristic for WT indeterminate nodules but in ZIII of Fix- nodules are devoid of rhizobia infected cells (lower images). The zones were labelled with square brackets and the IZ was highlighted in magenta. IZ, interzone; ZIId, distal part of infection zone; ZIII, nitrogen fixation zone; ZIIp, proximal part of infection zone. Bars: (a) 2 cm; (b) 200 μm.

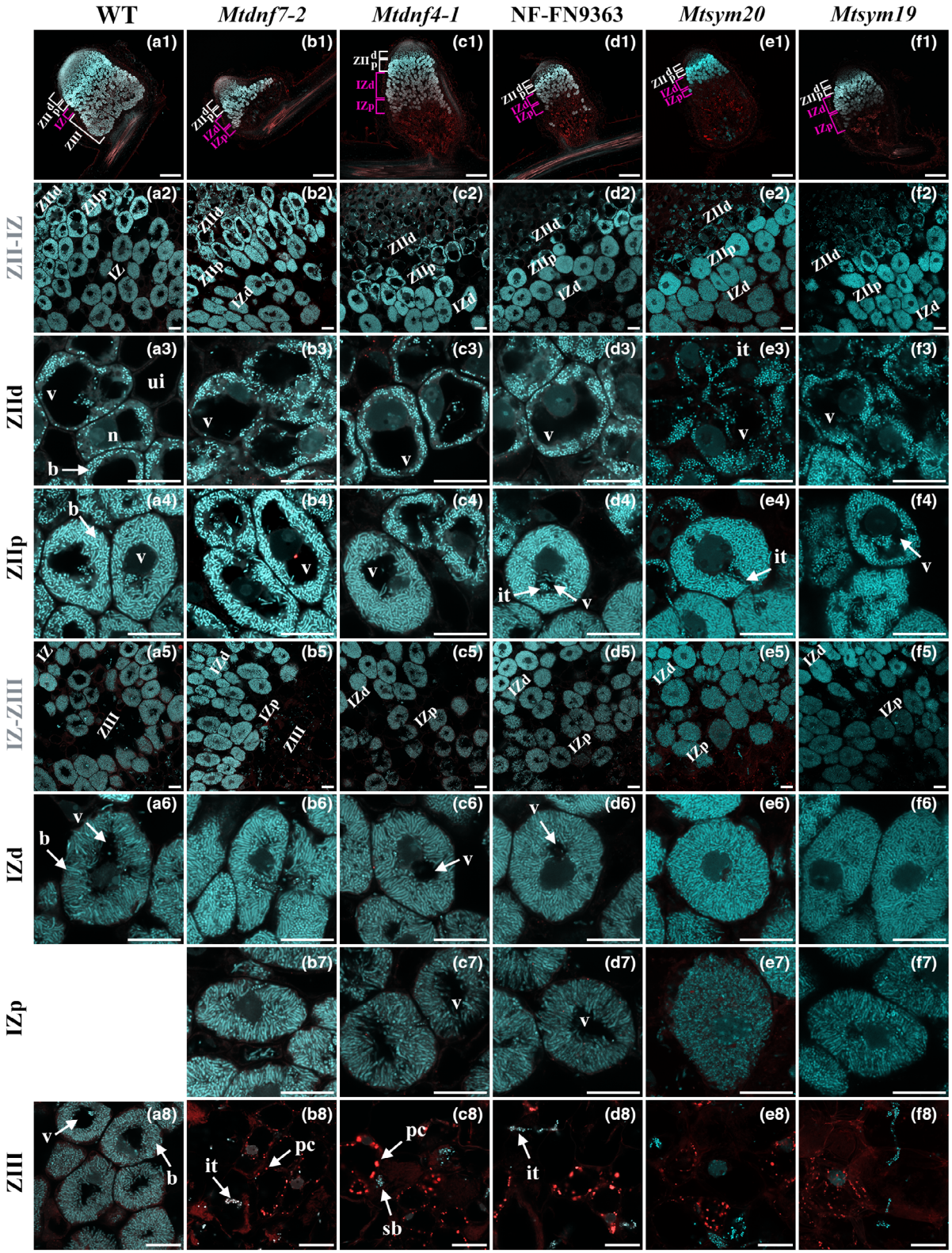

symbiotic form, was more extensive and enlarged in mutant nodules compared with WT nodules (Figs 1b, 2a1–f1). In contrast to WT nodules, the cells in nitrogen fixation zones of mutant nodules were not colonized by rhizobia but showed sporadic autofluorescence (Fig. 2b1–f1,b8–f8). Autofluorescence in nodule tissues often arises from phenolic compounds derived from pathogen-induced lignification that generally results in robust and extensive defence responses which were characteristics

Fig. 2 Laser confocal microscopic analyses of symbiotic cell structure and bacteroid morphology on SYTO13 stained nodule sections of the Fix- mutants NF-FN9363, *Mtsym19* and *Mtsym20* compared with nodules of WT and *Mtdnf7-2*, *Mtdnf4-1* plants 14 d post-inoculation with *Sinorhizobium medicae* WSM419. (a1–f1) SYTO13-stained longitudinal nodule sections show the defect of bacterial invasion in ZIII of ineffective symbiotic nodules. The green channel visualizes SYTO13-stained bacteroids and plant cell nuclei (cyan pseudo colour), autofluorescence is pseudo-coloured in red. Higher magnification shows the transition between ZII and IZ (a2–f2) and IZ–ZIII (a5–f5). (a3–f3, a4–f4) No obvious alteration was observed in bacterial occupation of infected cells or the morphology of bacteroids in distal part of ZII (ZIId) between WT and mutant nodule cells. (a6–f6; b7–f7) Moderate elongation of bacteroids was found in the proximal part of IZ (IZp) cells of mutant nodules compared with WT nodule cells. This region is composed of a single cell layer in WT nodules but it was extended in mutant nodules. Infected mutant cells in IZp contain disordered bacteroids indicating the inception of their disintegration. (a8–f8) The cells in ZIII but its first cell layer (IZp) in mutant nodules (b7–f7) were devoid of bacteroids and contained autofluoresced speckles indicating the presence of early senescence-related phenolic compounds. Bars: (a1–f1) 200 μm; (a2–f8) 20 μm. b, bacteroid; it, infection thread; IZ, interzone; IZd, distal part interzone; IZp, proximal part of interzone; n, nucleus; pc, phenolic compounds; sb, saprophytic bacteria; ui, uninfected cells; v, vacuole; ZIId, distal part of infection zone; ZIII, nitrogen fixation zone; ZIIp, proximal part of infection zone. White and magenta brackets indicate the extension of the zones.

of some *M. truncatula* symbiotic mutants (Bourcy *et al.*, 2013; Wang *et al.*, 2016; Domonkos *et al.*, 2017). By contrast, the early induced decomposing process, the premature senescence is frequently observed in ineffective symbiotic nodules (Van de Velde *et al.*, 2006). Early senescence generates less intensive and sporadic autofluorescence that was found previously in *Mtdnf4-1* and *Mtdnf7-2* nodules (Horvath *et al.*, 2015; Kim *et al.*, 2015). In addition to the difference in the extension and intensity between the defence-reactions and premature senescence-related autofluorescence, the two responses can be distinguished based on activation of marker genes specific for each process. The transcriptional activities of senescence and defence response-specific marker genes were monitored in the nodules of WT and mutant plants NF-FN9363, *Mtsym20*, *Mtdnf4*, *Mtdnf7-2* and *Mtnad1-3* (*nodules with activated defense 1–3*), in which the control of defence-like responses is deficient (Domonkos *et al.*, 2017), at 3 wpi using RT-qPCR. A strong induction of cysteine proteinase genes *MtCP2* and *MtCP6* associated with nodule senescence in *M. truncatula* (Guerra *et al.*, 2010) was detected in the ineffective symbiotic nodules of all studied mutants (Fig. S2a). By contrast, marker genes of defence responses, a chitinase (*MtCHI*) and *MtPR10* (Class-10 *PATHOGENESIS-RELATED PROTEIN*) genes were not induced in the mutants NF-FN9363, *Mtsym20*, *Mtdnf4* and *Mtdnf7-2* but showed high transcriptional activity in the mutant *Mtnad1-3* (Fig. S2b,c), indicating that the autofluorescence was the result of premature senescence in the nitrogen fixation zones of NF-FN9363, *Mtsym19*, *Mtsym20*, *Mtdnf4-1* and *Mtdnf7-2* nodules (Fig. 2b1–f8).

Higher magnification of SYTO13-stained nodule sections revealed that infected cells in ZII and IZ exhibited similar morphology in mutant and WT nodules (Fig. 2a1–f5). Bacterial release was normal in the distal part of ZII (ZIId) of mutant nodule cells and rhizobia commenced to differentiate in the proximal part of ZII (ZIIp). These nodule cells in ZIIp, characterized by moderately elongated rhizobia with intense fluorescence and enlarged vacuoles, were clearly visible in WT, *Mtdnf7-1* and *Mtdnf4-1* nodules but vacuole extension was less pronounced in nodules of FN9363, *Mtsym20* and *Mtsym19* (Fig. 2a4–f4). Cells in the first layer of the nitrogen fixation zone showed similar morphology, possessing compressed vacuoles, in WT and all mutant nodules although rhizobia were slightly shorter and disorganized in mutant symbiotic cells (Fig. 2a5–f6). Although this region is composed of a single layer of cells in WT nodules (Fig. 2a1; Gavrin *et al.*, 2014), we observed the extension of this part of nodules in all mutants (Fig. 2b1–f1) indicating the arrest of further differentiation of infected nodule cells. Differentiated bacteroids oriented towards the large vacuoles were observed in the nitrogen fixation zone of WT nodules (Fig. 2a6,a8). By contrast, vacuoles remained reduced in IZ cells of mutant nodules, resembling to the morphology of cells with compressed vacuoles in interzones (Fig. 2b7–f7). Mutant nodules did not contain infected cells in the region corresponding to the mature nitrogen fixation zone of WT nodules but sporadic autofluorescence and non-differentiated rod shape saprophytic bacteria released from the ITs were detected occasionally in this zone (Fig. 2a8–f8).

Bacteroid elongation and morphology are impaired in NF-FN9363 and *Mtsym20* nodules

Rhizobia undergo morphological changes including cell enlargement and genome amplification in the indeterminate nodules of *M. truncatula* resulting in elongated bacteroids (Mergaert *et al.*, 2006). The morphology of rhizobia in the interzone cells of mutant nodules indicated the impaired elongation of bacteroids (Fig. 2b5–f5). To determine the level of differentiation, the length and ploidy level of bacteria were measured. Bacteria were isolated from mutant and WT nodules 14 dpi, stained with propidium iodide (PI) and imaged by confocal laser scanning microscopy. The size of at least 1200 bacterial cells was measured using the ImageJ software and the relative ratio of bacteria in different size ranges was compared between WT and mutant nodules. Bacterial populations isolated from mutant nodules showed a shift to the smaller size range compared with WT sample indicating an imperfect elongation of bacteroids in *Mtdnf4-1*, *Mtdnf7-2*, NF-FN9363 and *Mtsym20* nodules (Fig. 3a).

The size and DNA content of rhizobia isolated from *Mtdnf4-1*, NF-FN9363 and *Mtsym20* mutant and WT nodules were further analysed by flow cytometry. Isolated bacteroids and cultured bacteria were purified and stained with PI. The analysis of forward scatter (FSC) intensity, that is proportional to the size of bacteroids, showed that the majority of bacteroids isolated from WT nodules were enlarged compared with cultured rhizobia (Fig. 3b). The bacterial population purified from mutant nodules contained a mixture of smaller sized cells peaked at the free-living rhizobia and at smaller sized bacteriods compared with WT samples. This finding was consistent with length measurements of bacteriods which showed the higher proportion of shorter rhizobia in mutant nodule cells compared with bacteria isolated from

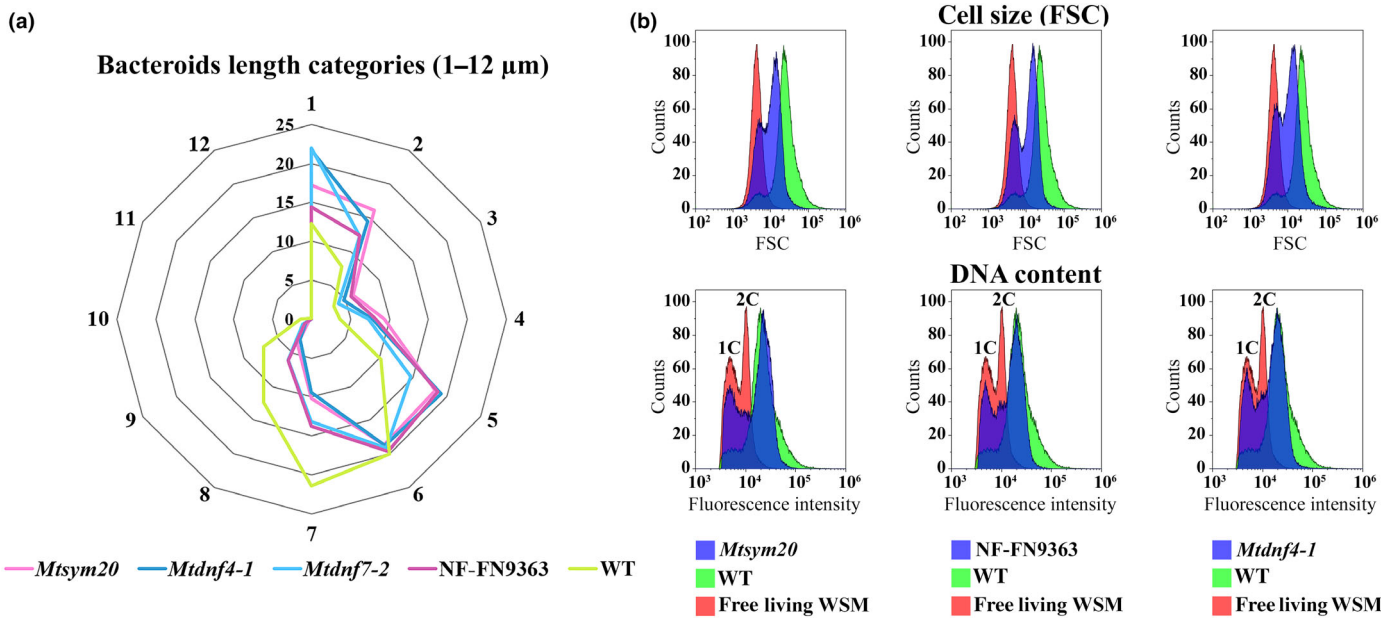

Fig. 3 Bacteroid differentiation is similarly impaired in NF-FN9363 and *Mtsym20* mutant nodules as in the formerly identified ineffective symbiotic mutants *Mtdnf4-1* and *Mtdnf7-2* at 2 wk post-inoculation (wpi) with *Sinorhizobium medicae* WSM419. (a) The distribution of size of bacteroids isolated from wild type (WT) and mutant nodules at 2 wpi, stained with propidium iodide (PI), captured by confocal laser scanning microscopy and measured on the images using the ImageJ program. The size of bacteroids from mutant nodules had a higher proportion of shorter bacterial cells compared with wild-types and rhizobia above 6 µm in length were hardly observed in mutant nodules although these classes in WT nodules were evident. The size of at least 1200 bacterial cells was measured and their relative distribution in length classes is presented. Values around the radar chart indicate bacterial length (µm) and circles show percentage (%). (b) The relative size and DNA content of *S. medicae* WSM419 bacteroids isolated from WT and mutant nodules at 16 d post-inoculation (dpi) measured by flow cytometry. Bacteroid relative size was determined by the forward light scatter (FSC) and endoreduplication was measured by fluorescence intensity. The size and DNA content of *S. medicae* WSM419 bacteroid populations isolated from mutant nodules shifted to smaller size and lower ploidy level compared with bacteroids found in WT nodules. 1C, DNA content of halpoid rhizobia genome; 2C, DNA content of replicated rhizobia genome.

WT nodules (Fig. 3a). The mean DNA content of bacteroids isolated from mutant nodules was higher than the peak of 1C or 2C ploidy levels of cultured *S. medicae* WSM419 cells indicating that bacteroids isolated from mutant nodules were polyploids (Fig. 3b). The peaks of the DNA content of rhizobia purified from mutant and WT nodules were very similar suggesting an advanced genome amplification of bacteroids in mutant nodules. However, the population of bacterial cells isolated from mutant nodules was narrower at a higher fluorescent range compared with rhizobia purified from WT nodules indicating less bacteroids with amplified genomes at the highest degree.

To detect alterations in mutant nodules in more detail, the ultrastructure of WT and NF-FN9363, *Mtsym20*, *Mtdnf4-1* and *Mtdnf7-2* nodules was analysed by SEM 18 dpi with *S. medicae* WSM419. Consistent with the light and fluorescent microscopy images, no visible difference was detected in the morphology and invasion of nodule cells in the distal part of ZII of WT and mutant nodules (Fig. S3a2–e3). However, a discontinuity between the rhizobia and plant cell walls was observed in the proximal part of IZ and the aggregation of bacteroids, often tangled with cell debris, and the collapse of symbiotic cells was more pronounced in ZIII of mutant nodules (Fig. S3b5–e6). These data reveal that rhizobia can differentiate to bacteroids in *Mtdnf4-1*, *Mtdnf7-2*, NF-FN9363 and *Mtsym20* nodules but their complete transition is either disrupted or the persistence of bacteroids is defective in mutant nodules.

Deletion of gene *NCR343* is responsible for the symbiotic defect of mutant NF-FN9363

Genetic mapping combined with exploiting the high-density genome array-based comparative genomic hybridization (aCGH) platform of *M. truncatula* (Chen *et al.*, 2017) was applied to identify the impaired genes in symbiotic mutant NF-FN9363. Genetic mapping positioned the mutant locus of NF-FN9363 on chromosome 6 (LG 6) below the genetic marker Crs towards MtB178 (Fig. S4a). To identify the gene defective in NF-FN9363, the genomic positions of copy number variations detected in the mutant line using the aCGH were analysed. A pile of probe sets corresponding to the genomic position of the symbiotic locus of NF-FN9363 indicated a potential large deletion in the mutant genome. The deletion was verified by PCR-based markers that defined an almost 500 kb deletion in the genome of NF-FN9363 (Figs 4a, S5; Table S1). The deletion in NF-FN9363 removed more than 30 predicted genes or gene models including four *NCR* genes, *NCR341*, *NCR343*, *NCR344* and *NCR345* which were the primary candidates responsible for the symbiotic phenotype of NF-FN9363 (Fig. S5b). All four *NCR* genes encode for peptides with four cysteines in conserved positions and the sequence analysis of the four mature NCR peptides revealed that NCR341, NCR344 and NCR345 showed higher similarity to each other compared with NCR343 (Fig. 4c). The most similar mature peptides of NCR341 and NCR344 are both cationic (pI = 8.67 and 7.95),

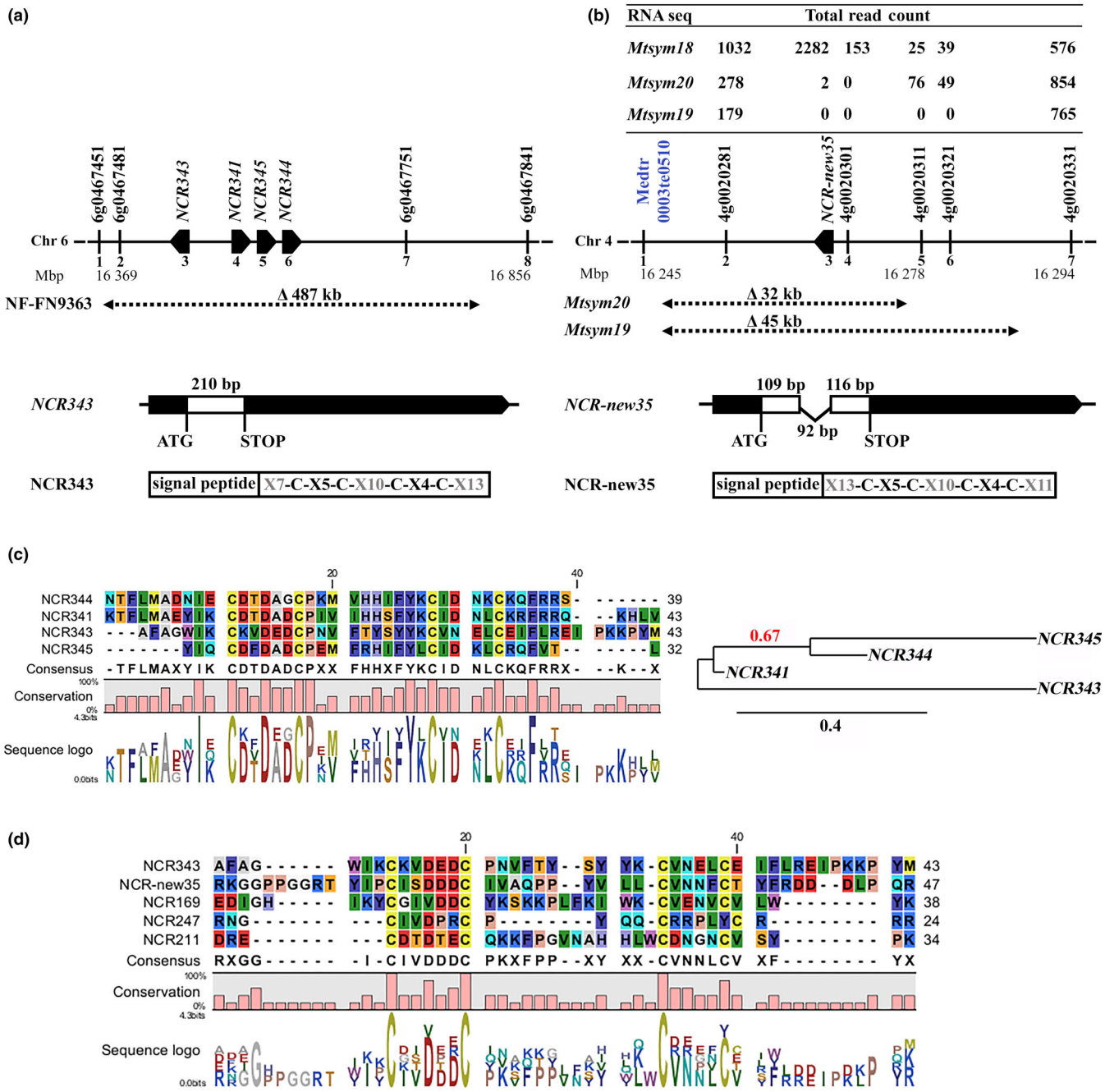

Fig. 4 The identified deleted regions and the gene models in the symbiotic loci of NF-FN9363 and *Mtsym19*, *Mtsym20* mutants. (a) Genetic mapping and high-density genome array-based comparative genomic hybridization (aCGH) identified a nearly 500 kb deletion including four *NCR* genes in the NF-FN9363 genome. (b) The extension of the deleted regions in the mutant loci of *Mtsym19* and *Mtsym20* was determined by PCR-based markers and by analysing reads obtained from RNAseq. The structure of the *NCR343* (a) and *NCR-new35* (b) genes (coding sequences, the intron of *NCR-new35* and 5′ UTRs and 3′ UTRs) are represented by white boxes, thin excised black line and thick black lines, respectively) and the features of the encoded NCR343 (a) and NCR-new35 (b) peptides containing a signal peptide and mature peptides with four cysteine residues in conserved positions. (c) Multiple sequence alignment and phylogenetic analysis of mature peptides encoded by the *NCR343*, *NCR341*, *NCR345* and *NCR344* genes deleted in the symbiotic locus of NF-FN9363 (0.67 indicates the branch support value using the standard bootstrap with 100 replicates and 0.4 bar scale indicates number of substitutions per site) and (d) the sequence analysis of mature NCR peptides proved to be crucial for differentiation and persistence of rhizobia during nitrogen-fixing symbiosis. The degree of sequence conservation of the residues between the four mature peptides is represented below the alignment. Colours are based on Robert Fletterick's 'Shapely models' (http://openrasmol.org/doc/rasmol.html#shapelycolours).

NCR345 is anionic (pI = 4.59), while NCR343 is slightly anionic (pI = 6.33). To point to the gene or genes responsible for the symbiotic phenotype of NF-FN9363, genetic complementation experiments were carried out. The genomic fragments of these four *NCR* genes were introduced into NF-FN9363 roots using *Agrobacterium rhizogenes*-mediated hairy-root transformation. Transformed

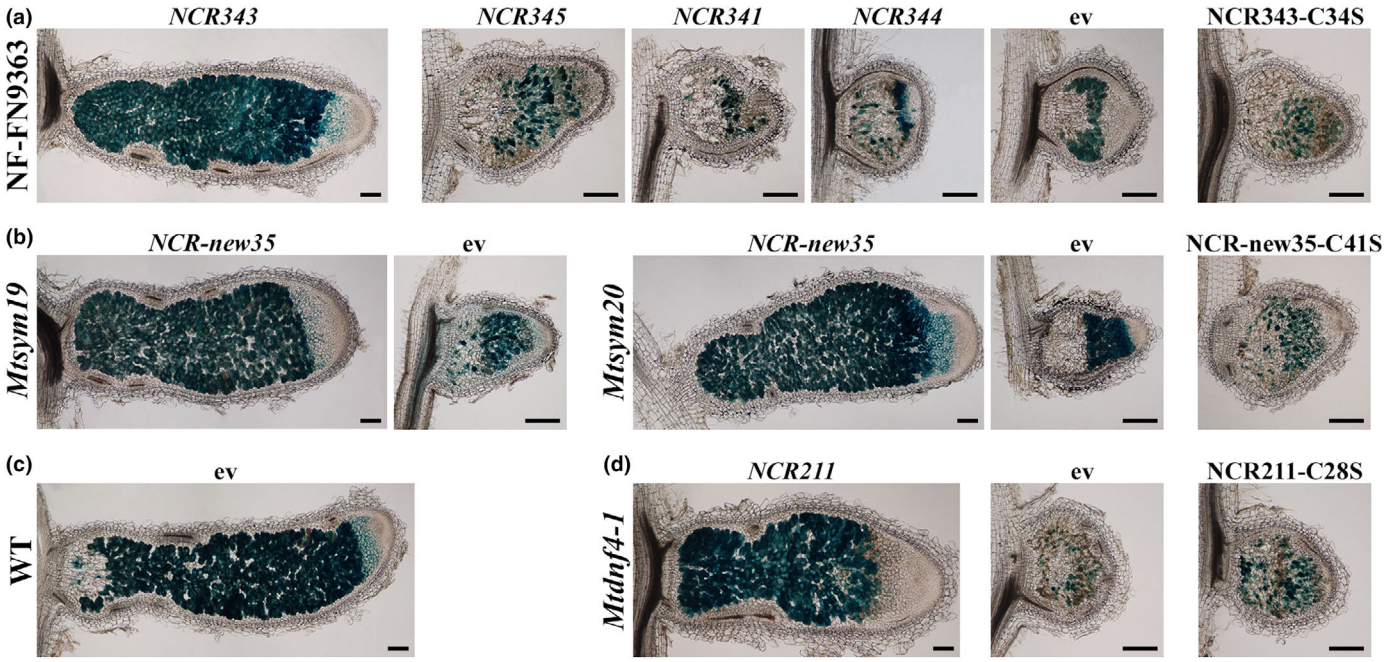

Fig. 5 *NCR343* and *NCR-new35* are required for development of functional nodules and the first cysteine residues of NCR343 and NCR-new35 peptides are essential for their function. The rescue of the nodulation defect of mutants NF-FN9363, *Mtsym19* and *Mtsym20* was identified based on the restoration of morphology and colonization of nodules formed on hairy roots transformed with empty vector (ev) or *NCR* peptide genes and inoculated with *Sinorhizobium medicae* WSM419 carrying the *lacZ* marker gene. Longitudinal sections of 4-wk-old nodules were stained for β-galactosidase activity. The nodules on NF-FN9363 roots transformed with *NCR343* (a), on *Mtsym19* and *Mtsym20* roots transformed with *NCR-new35* (b), on wild-type (WT) roots transformed with an empty vector (c) and on *Mtdnf4-1* roots transformed with *NCR211* genes (d) showed characteristic zonation of indeterminate nodules indicating the restoration of the symbiotic phenotypes. Gene constructs of *NCR345*, *NCR341*, and *NCR344* did not restore the symbiotic phenotype of nodules developed on transformed roots of NF-FN9363 indicating that these peptides are not essential for the symbiotic interaction between *Medicago truncatula* A17 and *S. medicae* WSM419. The substitution of the first cysteine residue for serine abolished complementation in the mutant NCR343 (a), NCR-new35 (b) and NCR211 (d) genes indicating the essential role of the first cysteines. Bar, 200 μm.

roots were detected by either DsRed or green fluorescent protein markers (Fig. S6). The roots were inoculated with *S. medicae* WSM419 (pXLGD4) and nodules were stained for β-galactosidase activity at 4 wpi. Nodule cells in nitrogen fixation zone of mutant NF-FN9363 were devoid of rhizobia (Fig. 1b); therefore, we assessed the complementation of nodules based on the presence of rhizobia in ZIII. White undeveloped nodules with colonized cells by rhizobia in ZII and IZ were detected on roots transformed with empty vector or with the genes *NCR341*, *NCR344* and *NCR345* indicating that these *NCR* genes were not able to restore the effective symbiotic interaction in NF-FN9363 (Figs 5a, S6g1–i3,l1–m). The nodules developed on the roots of NF-FN9363 transformed with the construct of *NCR343* were elongated and pink, and the bacterial invasion of ZIII in these nodules was like in WT, suggesting that these were functional nodules on NF-FN9363 roots (Figs 5a, S6f1–f3,k1–k3). The rescue of the symbiotic phenotype of NF-FN9363 with gene *NCR343* indicated that the loss of this gene caused the ineffective symbiotic phenotype of mutant NF-FN9363.

The lack of *NCR-new35* is responsible for the ineffective symbiotic phenotype of *Mtsym19* and *Mtsym20*

Genetic mapping facilitated with transcriptome analysis of symbiotic mutants was applied to identify the impaired genes in mutants *Mtsym19* and *Mtsym20*. The mutant loci of *Mtsym19* and *Mtsym20* were positioned in the same genomic region on chromosome 4 (LG 4) between genetic markers 4g0020111, 4g0020421 and 4g0020631 (Fig. S4a). Former genetic analysis suggested that *Mtsym19* and *Mtsym20* belong to different complementation groups (Morandi *et al.*, 2005). However, the similar position of the mutant loci of *Mtsym19* and *Mtsym20* indicated either the defect of two different neighbouring genes or the malfunction of the same gene in the two mutants. To verify their allelic relationship, an allelism test was carried out using F3 mutant plants selected from the mapping populations. The allelism test revealed that *Mtsym19* and *Mtsym20* belong to the same complementation group (Fig. S4b).

To facilitate the identification of impaired gene in *Mtsym19* and *Mtsym20*, the transcript abundance in nodules of *Mtsym19*, *Mtsym20* and the symbiotic mutant *Mtsym18*, belonging to an independent symbiotic complementation group (Morandi *et al.*, 2005), was analysed at 2 wpi with *S. medicae* WSM419. Filtered sequence reads were mapped against the *M. truncatula* genome assembly (A17r5.0) and the number of reads was analysed in the genomic region between genetic markers 4g0020111 and 4g0020631. Absent or reduced number of reads aligned to a short non-specific sequence were detected between gene models 4g0020281 and 4g0020321 in *Mtsym19*, and between 4g0020281 and 4g0020301in *Mtsym20* compared with *Mtsym18*, indicating

deletions in these genomic regions (Figs 4b, S7a). Further analysis by PCR amplifications identified a < 45-kb and a < 32 kb deletion in the *Mtsym19* and *Mtsym20* genomes, respectively. The deletion in *Mtsym20* spanned three genes encoding for two putative proteins and a NCR peptide (Fig. S7b).

The identified deletions in mutants *Mtsym19* and *Mtsym20* overlapped by *c.* 32 kb removing three genes including the gene *NCR-new35*, formerly termed *NCR014* (de Bang *et al.*, 2017) but renamed according to the recent genome release of *M. truncatula* (Mt5.0; Figs 4b, S7b; Jardinaud *et al.*, 2022), which made *NCR-new35* the best candidate for *MtSYM19* and *MtSYM20*. To confirm that the deletion of *NCR-new35* caused the ineffective symbiotic phenotype of *Mtsym19* and *Mtsym20*, roots of the two mutants were transformed with the WT *NCR-new35* gene and inoculated with *S. medicae* WSM419 (pXLGD4). DsRed-fluorescent transgenic *Mtsym19* and *Mtsym20* roots expressing the gene *NCR-new35* developed elongated and pink nodules (Fig. S6b1–b3,d1-d3,o1–o3) in contrast to white round-shaped or slightly cylindrical nodules formed on empty vector-transformed roots of mutant plants (Fig. S6c1–c3,e1–e3,p1–p3). In order to visualize bacterial invasion, longitudinal sections of 4-wk-old nodules were stained for β-galactosidase activity. Rhizobia-colonized cells were observed only in zones II and IZs of nodules formed on empty vector-transformed *Mtsym19* and *Mtsym20* roots (Fig. 5b). Nodules developed on mutant roots transformed with the *NCR-new35* construct showed the typical zonation of indeterminate nodules with colonized cells in ZIII like nodules on empty vector-transformed WT roots (Figs 5b,c, S6a1–a3,j1–j3). The restoration of nodule colonization in ZIII of mutant nodules confirmed that gene *NCR-new35* corresponds to *MtSYM19* and *MtSYM20*.

Replacement of a single cysteine residue in NCR211, NCR343 and NCR-new35 abolishes their symbiotic function

NCR peptides usually contain four or six cysteine residues in conserved positions (Alunni *et al.*, 2007). We demonstrated previously that the replacement of a single or multiple cysteine residues of the symbiotic peptide NCR169 ceased its activity *in planta* indicating that each cysteine residue is essential for the symbiotic function of NCR169 (Horvath *et al.*, 2015). To confirm the requirement of cysteine residues for the function of NCR-new35, NCR343 and NCR211, we introduced constructs coding for modified peptides, wherein the first cysteines were substituted for serines, into the roots of *Mtsym20*, NF-FN9363 and *Mtdnf4-1* plants, respectively, using *A. rhizogenes*-mediated hairy-root transformation. The nodules on the roots of mutants transformed with the modified *NCRs* driven by their native promoters were small and white, suggesting that these were malfunctioning nodules (Figs 5, S6). These nodules did not show the typical zonation of indeterminate nodules and nodule regions proximal to the root corresponding to ZIII were devoid of bacteria, indicating that the first cysteine residues are essential for the function of NCR-new35, NCR343 and NCR211.

NCR-new35 is expressed low in symbiotic cells compared with *NCR169*, *NCR211* and *NCR343*

The members of the large family of *NCR* genes in *M. truncatula* are almost exclusively expressed in symbiotic nodule cells and they are activated in successive waves during nodule differentiation (Guefrachi *et al.*, 2014). To investigate the expression of *NCR-new35* and *NCR343*, their activity was monitored with the *GUS* reporter gene and RT-qPCR analysis, and we also analysed the nodule transcriptome data of different *M. truncatula* nodule zones obtained by laser-capture microdissection (LCM; Roux *et al.*, 2014).

To analyse and compare the expression pattern of *NCR-new35* and *NCR343* with the previously identified *NCR169* and *NCR211* genes essential for effective nitrogen fixation (Horvath *et al.*, 2015; Kim *et al.*, 2015), the promoters of these *NCR* genes were fused to the β-glucuronidase (*GUS*) reporter gene and the constructs were introduced into WT *M. truncatula* roots using *A. rhizogenes*-mediated hairy-root transformation. Histochemical staining of nodules for GUS activity was analysed at 2 and 3 wpi with *S. medicae* WSM419. *NCR343*, *NCR211* and *NCR169* promoters showed activity predominantly in the interzone of 2-wk-old nodules (Fig. 6c–e). By contrast, a low level of *GUS* expression was restricted mainly to the first few cell layers of the interzone and even weaker activity was found sporadically in the distal part of nitrogen fixation zone when the reporter gene was driven by the promoter of *NCR-new35* (Fig. 6b). The activity of these promoters is in agreement with LCM data (Roux *et al.*, 2014), confirming that *NCR-new35*, *NCR343*, *NCR211* and *NCR169* are mainly active in the IZs of 2-wk-old nodules and *NCR-new35* is expressed at a much lower level compared with the other three *NCR* genes (Fig. 6). The analysis of the promoter activities with the *GUS* reporter gene at 3 wpi revealed that the expression of *NCR169* and *NCR343* and to a lesser extent the activity of *NCR211* extended into the nitrogen fixation zone (Fig. 6g–j). To further validate their expression in nodules, we monitored the transcript levels of *NCR-new35*, *NCR343*, *NCR211* and *NCR169* with RT-qPCR in nodules harvested at 2 and 3 wpi. In agreement with the LCM transcriptome data, *NCR343*, *NCR211* and *NCR169* genes showed high relative expression compared with *NCR-new35* (Fig. 6k). These transcriptome and *GUS* activity data indicate that *NCR-new35* shows different spatial activity and lower expression intensity compared with the other three essential NCR peptide genes.

NCR-new35 and NCR343 peptides localize to symbiosomes

NCR peptides usually have a conserved signal peptide which cleavage is essential for targeting of NCR peptides to the bacteroids (Van de Velde *et al.*, 2010; Wang *et al.*, 2010). Previous studies demonstrated the localization of NCR169 and NCR211 peptides to the bacteroids in the symbiotic cells in the IZ and ZIII (Horvath *et al.*, 2015; Kim *et al.*, 2015). To explore the subcellular localization of NCR-new35 and NCR343 peptides, translational fusions to the *mCherry* reporter gene driven by native *NCR-new35*

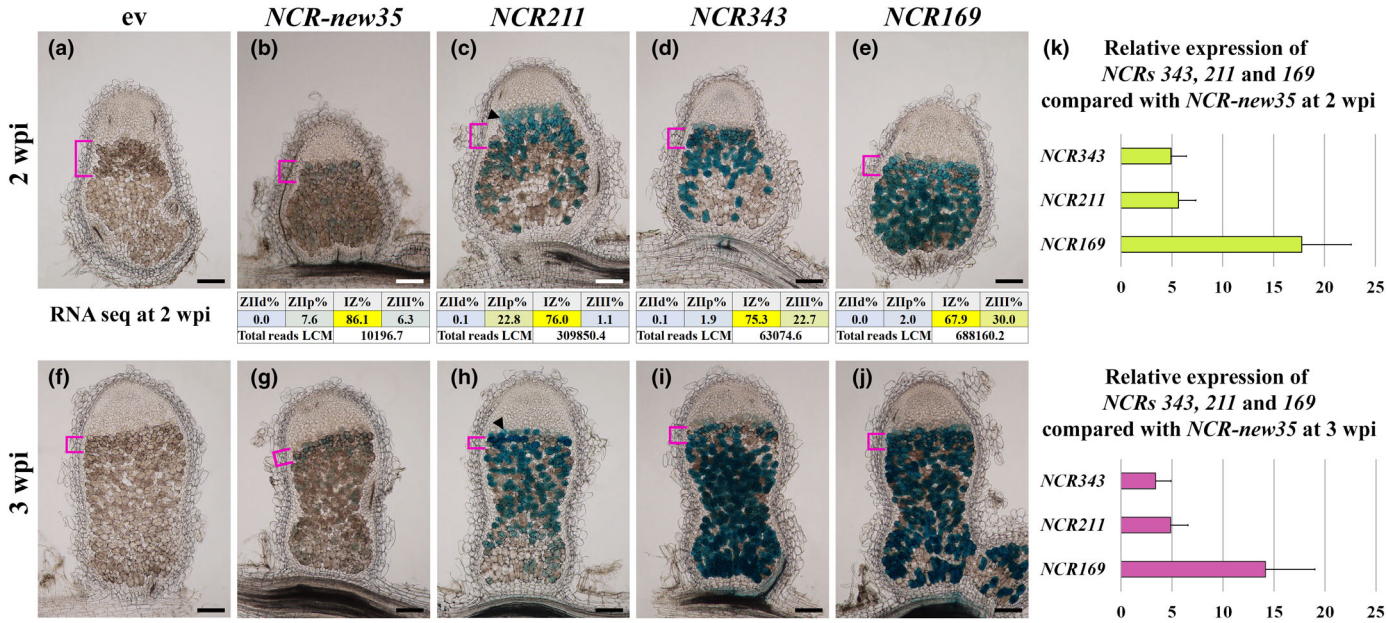

Fig. 6 The expression analysis of the *NCR-new35* and *NCR343* genes is compared with the activity of *NCR211* and *NCR169*. The empty vector (ev) (a, f) and the construct of promoter fragments of *NCR-new35* (b, g), *NCR211* (c, h), *NCR343* (d, i) and *NCR169* (e, j) genes fused to the β-glucoronidase (GUS) gene, respectively, were introduced into the roots of wild type (WT) Jemalong plants with *Agrobacterium rhizogenes*-mediated hairy-root transformation. Nodule sections were stained for GUS activity at 2 (a–e) and 3 (f–j) wk post-inoculation (wpi) with *Sinorhizobium medicae* WSM419. The relative spatial expression of *NCR-new35*, *NCR211*, *NCR343* and *NCR169* genes 2 wpi with *S. medicae* WSM419 generated with RNA sequencing of different nodule zones obtained with laser-capture microdissection (LCM) are shown below the images of 2-wk-old nodules. (k) Relative expression of *NCR169*, *NCR211* and *NCR343* compared with *NCR-new35* was analysed in WT nodules by reverse transcription quantitative polymerase chain reaction (RT-qPCR) 2 and 3 wpi with rhizobia. The relative expression of *NCR* genes is set to 1 for *NCR-new35*. Magenta square brackets, IZ, interzone; black arrowhead, ZIId, distal part of infection zone; ZIII, nitrogen fixation zone; ZIIp, proximal part of infection zone. Bar, 200 μm. Error bars indicate SE.

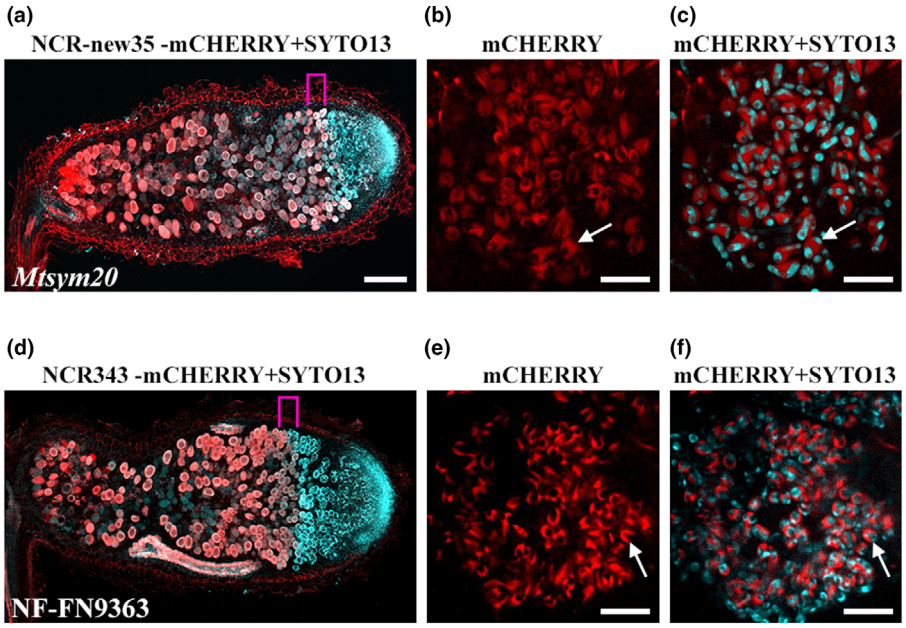

Fig. 7 NCR-new35-mCherry and NCR343-mCherry fusion proteins restored the symbiotic defects of *Mtsym20* (a) and NF-FN9363 (d) mutant plants, respectively, at 4 wk post-inoculation (wpi) with *Sinorhizobium medicae* WSM419. (a, d) The red NCR-new35-mCherry and NCR343-mCherry signals overlap with the fluorescence of SYTO13-stained bacteroids (cyan pseudo-colour) in the infected cells of interzones (magenta brackets) and nitrogen fixation zones indicating the co-localization of bacteroids and peptides NCR-new35 and NCR343. (b, c, e, f) Higher magnification of cells from the IZ revealed the red mCherry signal of NCR-new35 and NCR343 fusion proteins surrounding the bacteroids in the peribacteroid space (white arrows). IZ, interzone; Bars: (a, d) 200 μm; (b, c, e, f) 20 μm.

or *NCR343* promoters were generated and introduced into *Mtsym20* and NF-FN9363 mutant roots, respectively using hairy-root transformation. The functional complementation of the mutant nodules indicated that the fusion proteins retained their activity and the fluorescent tag did not perturb the function of NCR-new35-mCherry and NCR343-mCherry proteins (Fig. 7). The red fluorescence of NCR-new35-mCherry and NCR343-mCherry proteins was detected in the IZ and nitrogen fixation zone. The signal of the NCR-new35-mCherry fusion protein is partially contradictory to the expression pattern of *NCR-new35*

detected at 3 wpi with rhizobia (Fig. 6g) and points to the sustained stability of the NCR-new35-mCherry fusion protein in ZIII. In contrast to NCR-new35-mCherry, the subcellular localization of NCR343-mCherry corresponded completely to the spatial expression pattern of *NCR343* (Fig. 6i). Higher magnification of symbiotic cells showed that mCherry-tagged NCR-new35 and NCR343 fusion proteins surrounded the SYTO13-stained rhizobia (Fig. 7c,f).

Discussion

The *M. truncatula* genome contains *c.* 700 *NCR* genes which are almost exclusively expressed in symbiotic nodule cells (Guefrachi *et al.*, 2014; Roux *et al.*, 2014). The encoded NCR peptides mediate terminal differentiation of rhizobia (Van de Velde *et al.*, 2010) but the high number of *NCR* genes raises the question of why *M. truncatula* evolved so many genes and how many of them are required for the establishment of symbiotic nitrogen fixation. Forward and reverse genetic analysis identified that peptides NCR169, NCR211 and NCR247 are crucial for effective nitrogen-fixing symbiosis (Horvath *et al.*, 2015; Kim *et al.*, 2015; Sankari *et al.*, 2022) which prompted us to continue the analysis of ineffective *M. truncatula* symbiotic mutants to identify further essential *NCR* genes. Based on the nodulation phenotype of mutants defective in genes *NCR169*, *NCR211* and *NCR247*, we focused on symbiotic mutants *Mtsym19*, *Mtsym20* and NF-FN9363 that developed slightly elongated white nodules with zonation and invaded nodule cells in the distal part of the nodules. The histological analysis revealed that nodule zonation and the morphology of cells in the infection and the transition zones of mutant nodules were very similar to WT nodules indicating the formation of differentiated symbiotic cells in mutant nodules. However, the extended transition zone in mutant nodules compared with WT nodules indicated a defect in the differentiation process. This is in agreement with a former study detecting a higher ploidy level of nodule cells in *Mtsym19* and *Mtsym20* mutants compared with TE7 mutant, which is defective in the *IPD3* gene (Horvath *et al.*, 2011; Ovchinnikova *et al.*, 2011) having non-differentiated symbiotic nodule cells, but *Mtsym19* and *Mtsym20* nodule cells had lower endoreduplication index than WT nodules (Maunoury *et al.*, 2010). The analysis of the length and DNA content of bacteroids isolated from *Mtsym19*, *Mtsym20* and NF-FN9363 nodules showed that mutant nodules contained lower proportion of longer and endoreduplicated bacteroids compared with WT nodules. These results indicated that the differentiation of nodule cells and hosted bacteroids was advanced but not complete in *Mtsym19*, *Mtsym20* and NF-FN9363. This finding was in accordance with the histological and transcriptome analysis of *Mtsym19* and *Mtsym20* nodules which detected the activation of a second transcriptome-switch characteristic of late Fix- mutant plants (Maunoury *et al.*, 2010). The expression analysis of senescence and defence-related marker genes suggests that the failure of colonization of the cells in the mature part of ZIII and thus the absence of effective nitrogen fixation in mutant nodules induced premature senescence of symbiotic cells.

The deletion in the NF-FN9363 mutant includes four *NCR* genes in proximity. *NCR341*, *NCR343*, *NCR344* and *NCR345* showed high similarity at amino acid level which implies that these homologues have recently evolved by tandem duplication. However, only NCR343 can restore the symbiotic phenotype of NF-FN9363 indicating a specialization of this peptide for the symbiotic interaction between *M. truncatula* cv Jemalong and the tested rhizobia. Further analysis by exchanging residues or fragments between NCR341, NCR343, NCR344 and NCR345 peptides could reveal the unique region(s) of NCR343 responsible for its distinct biological function. The identified deletions in *Mtsym19* and *Mtsym20* overlapped indicating that they are defective in the same gene which is in contradiction to the previous allelism test that defined them as being in distinct complementation groups (Morandi *et al.*, 2005). Our allelism test and complementation experiments with gene *NCR-new35* clearly confirmed that *Mtsym19* and *Mtsym20* are allelic.

The spatial expression analysis of crucial *NCR* genes identified by forward genetic approach (Horvath *et al.*, 2015; Kim *et al.*, 2015 and this study) was analysed by a GUS-reporter assay which showed that *NCR169*, *NCR211* and *NCR343* are active in the infected cells of IZ and ZIII but detected the expression *NCR-new35* principally in IZ cells. This observation is in correlation with RNA sequencing data obtained from laser-capture microdissected nodule zones (Roux *et al.*, 2014). In addition, the expression of *NCR-new35* was much weaker compared with the other three *NCR* genes suggesting that the transcriptional intensity of an *NCR* gene does not correlate with its necessity for symbiosis. Although the promoter activity of *NCR-new35* is barely detectable in nitrogen fixation zone, the encoded peptide is abundant in this zone suggesting a slow turnover or the enhanced stability of NCR-new35. Formerly, the identification of several NCR peptides, which are expressed during the early stages of nodule colonization, in mature bacteroids suggested the sustained stability of these NCR peptides (Durgo *et al.*, 2015). Correspondingly to the previous finding on NCR169 peptide (Horvath *et al.*, 2015), both NCR343 and NCR-new35 co-localize with bacteroids forming a ring-shaped fluorescent signal. Apparently, the fluorescent protein fusions of NCR peptides, which are functional and able to rescue the symbiotic phenotype of the corresponding mutants, are localized around the bacteroids. However, a previous proteomic study identified NCR343 and NCR169, but not NCR211 and NCR-new35, in bacteroids (Durgo *et al.*, 2015) indicating that at least a subset of the fluorescent-tagged NCR fusion molecules, conceivably following proteolytic cleavage, enter the bacteroids.

The *NCR343* gene consists of one exon but *NCR-new35* has two exons, which is the most common gene structure of *M. truncatula NCR* genes. The encoded mature peptides are composed of 43 and 47 amino acids, respectively, including four cysteine residues at conserved positions, the characteristic feature of *M. truncatula* NCR peptides. The charge of the mature peptides is slightly or strongly anionic (isoeletric point (pI) = 6.34 for NCR343 and 4.78 for NCR-new35). The charges of the five NCR peptides (NCR169 pI = 8.45, NCR211 pI = 5.38, NCR247 pI = 10.15, NCR343 and NCR-new35) proved to be

essential for symbiosis vary between 4.78 and 10.15 indicating that anionic, neutral and cationic NCR peptides could be essential for nitrogen-fixing symbiosis in *M. truncatula*. The formation of intramolecular disulphide bonds between the conserved cysteine residues in NCR044 and NCR169 peptides was experimentally verified (Velivelli *et al.*, 2020; Isozumi *et al.*, 2021) and the *in planta* functional requirement of cysteine residues was demonstrated with substitution of cysteines with serines which resulted in inactivation of NCR169 (Horvath *et al.*, 2015). The replacement of the first cysteine residue with serine in NCR343 and NCR-new35 also abolished the symbiotic activity of the peptides implying that the requirement of cysteine residues for the *in planta* activity is a common feature of NCRs. Apart from the four cysteine residues in conserved positions, the five crucial NCR peptides show high sequence variation but the presence of a valine, an isoleucine and one or two aspartic acid residues between the first two cysteines is dominant (Fig. 4d). The relevance of these residues for the structure and symbiotic activity of NCR peptides requires further investigation.

Based on the observation that terminally differentiated bacteroids are symbiotically more effective compared with reversibly differentiated ones (Oono & Denison, 2010), it is widely accepted that the controlled bacteroid growth in nodules provides increased fitness benefits for the host. In IRLC legumes and some Dalbergoid legume species, rhizobia undergo terminal differentiation provoked by NCR peptides (see reviews Czernic *et al.*, 2015; Pan & Wang, 2017; Downie & Kondorosi, 2021). The large number of *NCR* genes of *M. truncatula* induced in consecutive steps and showing overlap expression which implies that these peptides might function together to optimize the interaction between rhizobia and the host, and potentially some of them compensate the negative effect of other NCR peptides (Mergaert, 2018). It has been presumed that there is a core set of *M. truncatula* NCRs with common functions, and their loss results in the termination of bacteroid differentiation and/or losing the viability of hosted rhizobia (Pan & Wang, 2017; Roy *et al.*, 2020). Till now NCR169, NCR211 and NCR247 were identified as essential peptides for symbiosis but our work provides two additional ones, NCR343 and NCR-new35 required for effective nitrogen fixation between *M. truncatula* and *Sinorhizobium* species. The identification of novel crucial NCRs implies that further forward and reverse genetic studies might extend the cluster of universal and essential NCR peptides of *M. truncatula*.

Acknowledgements

This work was supported by the Hungarian National Research Fund/National Research, Development and Innovation Office grants OTKA-67576, PD104334/108923, 106068, 119652 and 120122/120300, PD-121110 and PD-132495 as well as by the Collaborative Research Programme ICGEB Research Grant HUN17-03. The present work has benefited from Imagerie-Gif core facility supported by l'Agence Nationale de la Recherche (ANR-11-EQPX-0029/Morphoscope, ANR-10-INBS-04/FranceBioImaging; ANR-11-IDEX-0003-02/Saclay Plant Sciences). FA received funding from H2020 (SGA no. 739593). We thank H. Cs. Tolnainé for her skilful technical assistance and A. Farkas for carrying out sample preparation SEM imaging.

Competing interests

None declared.

Author contributions

BH, ÁD, RC and PK designed the project. BH, BG, MT, ÁD, FA, FS, YC, MB, JBB and ZT performed the experiments. ÁD and ZS carried out data analysis. PK wrote the manuscript. BH and BG contributed equally to this work.

ORCID

Ferhan Ayaydin https://orcid.org/0000-0002-9126-0865
János Barnabás Biró https://orcid.org/0000-0001-8851-0387
Mickael Bourge https://orcid.org/0000-0002-4111-6208
Rujin Chen https://orcid.org/0000-0001-5444-2144
Yuhui Chen https://orcid.org/0000-0002-8831-8501
Ágota Domonkos https://orcid.org/0000-0003-4017-0605
Berivan Güngör https://orcid.org/0000-0002-5612-1130
Beatrix Horváth https://orcid.org/0000-0001-8499-568X
Péter Kaló https://orcid.org/0000-0002-0404-8904
Farheen Saifi https://orcid.org/0000-0002-6912-8227
Zoltán Szabó https://orcid.org/0000-0002-2001-0375
Zoltán Tóth https://orcid.org/0000-0002-3212-2438

Data availability

All data supporting the findings of this study are available within the paper and within its supplementary materials published online.

References

Alunni B, Kevei Z, Redondo-Nieto M, Kondorosi A, Mergaert P, Kondorosi E. 2007. Genomic organization and evolutionary insights on GRP and NCR genes, two large nodule-specific gene families in *Medicago truncatula*. *Molecular Plant–Microbe Interactions* **20**: 1138–1148.

de Bang TC, Lundquist PK, Dai XB, Boschiero C, Zhuang ZH, Pant P, Torres-Jerez I, Roy S, Nogales J, Veerappan V *et al.* 2017. Genome-wide identification of *Medicago* peptides involved in macronutrient responses and nodulation. *Plant Physiology* **175**: 1669–1689.

Boivin C, Camut S, Malpica C, Truchet G, Rosenberg C. 1990. *Rhizobium meliloti* genes encoding catabolism of trigonelline are induced under symbiotic conditions. *Plant Cell* **2**: 1157–1170.

Bourcy M, Brocard L, Pislariu CI, Cosson V, Mergaert P, Tadege M, Mysore KS, Udvardi MK, Gourion B, Ratet P. 2013. *Medicago truncatula* DNF2 is a PI-PLC-XD-containing protein required for bacteroid persistence and prevention of nodule early senescence and defense-like reactions. *New Phytologist* **197**: 1250–1261.

Chen YH, Wang XF, Lu SF, Wang HC, Li SB, Chen RJ. 2017. An array-based comparative genomic hybridization platform for efficient detection of copy number variations in fast neutron-induced *Medicago truncatula* Mutants. *Journal of Visualized Experiments* **8**: 56470.

Czernic P, Gully D, Cartieaux F, Moulin L, Guefrachi I, Patrel D, Pierre O, Fardoux J, Chaintreuil C, Nguyen P *et al.* 2015. Convergent evolution of endosymbiont differentiation in dalbergioid and inverted repeat-lacking clade

legumes mediated by nodule-specific cysteine-rich peptides. *Plant Physiology* **169**: 1254–1265.

Domonkos A, Horvath B, Marsh JF, Halasz G, Ayaydin F, Oldroyd GED, Kalo P. 2013. The identification of novel loci required for appropriate nodule development in *Medicago truncatula*. *BMC Plant Biology* **13**: 157.

Domonkos A, Kovacs S, Gombar A, Kiss E, Horvath B, Kovats GZ, Farkas A, Toth MT, Ayaydin F, Boka K *et al.* 2017. NAD1 controls defense-like responses in *Medicago truncatula* symbiotic nitrogen fixing nodules following rhizobial colonization in a BacA-independent manner. *Genes* **8**: e387.

Downie JA, Kondorosi E. 2021. Why should nodule cysteine-rich (NCR) peptides be absent from nodules of some groups of legumes but essential for symbiotic N-fixation in others? *Frontiers in Agronomy* **3**: 654576.

Durgo H, Klement E, Hunyadi-Gulyas E, Szucs A, Kereszt A, Medzihradszky KF, Kondorosi E. 2015. Identification of nodule-specific cysteine-rich plant peptides in endosymbiotic bacteria. *Proteomics* **15**: 2291–2295.

Gavrin A, Kaiser BN, Geiger D, Tyerman SD, Wen ZY, Bisseling T, Fedorova EE. 2014. Adjustment of host cells for accommodation of symbiotic bacteria: vacuole defunctionalization, HOPS suppression, and TIP1g retargeting in *Medicago*. *Plant Cell* **26**: 3809–3822.

Guefrachi I, Nagymihaly M, Pislariu CI, de Velde WV, Ratet P, Mars M, Udvardi MK, Kondorosi E, Mergaert P, Alunni B. 2014. Extreme specificity of NCR gene expression in *Medicago truncatula*. *BMC Genomics* **15**: 712.

Guerra J, Coussens G, De Keyser A, De Rycke R, De Bodt S, Van De Velde W, Goormachtig S, Holsters M. 2010. Comparison of developmental and stress-induced nodule senescence in *Medicago truncatula*. *Plant Physiology* **152**: 1574–1584.

Hirsch AM. 1992. Developmental biology of legume nodulation. *New Phytologist* **122**: 211–237.

Horvath B, Domonkos A, Kereszt A, Szucs A, Abraham E, Ayaydin F, Boka K, Chen YH, Chen RJ, Murray JD *et al.* 2015. Loss of the nodule-specific cysteine rich peptide, NCR169, abolishes symbiotic nitrogen fixation in the *Medicago truncatula dnf7* mutant. *Proceedings of the National Academy of Sciences, USA* **112**: 15232–15237.

Horvath B, Yeun LH, Domonkos A, Halasz G, Gobbato E, Ayaydin F, Miro K, Hirsch S, Sun JH, Tadege M *et al.* 2011. *Medicago truncatula* IPD3 is a member of the common symbiotic signaling pathway required for rhizobial and mycorrhizal symbioses. *Molecular Plant–Microbe Interactions* **24**: 1345–1358.

Isozumi N, Masubuchi Y, Imamura T, Mori M, Koga H, Ohki S. 2021. Structure and antimicrobial activity of NCR169, a nodule-specific cysteine-rich peptide of *Medicago truncatula*. *Scientific Reports* **11**: 9923.

Jardinaud MF, Fromentin J, Auriac MC, Moreau S, Pecrix Y, Taconnat L, Cottret L, Aubert G, Balzergue S, Burstin J *et al.* 2022. MtEFD and MtEFD2: two transcription factors with distinct neofunctionalization in symbiotic nodule development. *Plant Physiology* **189**: 1587–1607.

Jones KM, Kobayashi H, Davies BW, Taga ME, Walker GC. 2007. How rhizobial symbionts invade plants: the *Sinorhizobium-Medicago* model. *Nature Reviews Microbiology* **5**: 619–633.

Kim M, Chen YH, Xi JJ, Waters C, Chen RJ, Wang D. 2015. An antimicrobial peptide essential for bacterial survival in the nitrogen-fixing symbiosis. *Proceedings of the National Academy of Sciences, USA* **112**: 15238–15243.

Kovacs S, Fodor L, Domonkos A, Ayaydin F, Laczi K, Rakhely G, Kalo P. 2021. Amino acid polymorphisms in the VHIID conserved motif of nodulation signaling pathways 2 distinctly modulate symbiotic signaling and nodule morphogenesis in *Medicago truncatula*. *Frontiers in Plant Science* **12**: 709857.

Maunoury N, Redondo-Nieto M, Bourcy M, Van de Velde W, Alunni B, Laporte P, Durand P, Agier N, Marisa L, Vaubert D *et al.* 2010. Differentiation of symbiotic cells and endosymbionts in *Medicago truncatula* nodulation are coupled to two transcriptome-switches. *PLoS ONE* **5**: e9519.

Mergaert P. 2018. Role of antimicrobial peptides in controlling symbiotic bacterial populations. *Natural Product Reports* **35**: 336–356.

Mergaert P, Nikovics K, Kelemen Z, Maunoury N, Vaubert D, Kondorosi A, Kondorosi E. 2003. A novel family in *Medicago truncatula* consisting of more than 300 nodule-specific genes coding for small, secreted polypeptides with conserved cysteine motifs. *Plant Physiology* **132**: 161–173.

Mergaert P, Uchiumi T, Alunni B, Evanno G, Cheron A, Catrice O, Mausset AE, Barloy-Hubler F, Galibert F, Kondorosi A *et al.* 2006. Eukaryotic control on bacterial cell cycle and differentiation in the Rhizobium-legume symbiosis. *Proceedings of the National Academy of Sciences, USA* **103**: 5230–5235.

Montiel J, Downie JA, Farkas A, Bihari P, Herczeg R, Balint B, Mergaert P, Kereszt A, Kondorosi E. 2017. Morphotype of bacteroids in different legumes correlates with the number and type of symbiotic NCR peptides. *Proceedings of the National Academy of Sciences, USA* **114**: 5041–5046.

Morandi D, Prado E, Sagan M, Duc G. 2005. Characterisation of new symbiotic *Medicago truncatula* (Gaertn.) mutants, and phenotypic or genotypic complementary information on previously described mutants. *Mycorrhiza* **15**: 283–289.

Nagymihaly M, Veluchamy A, Gyorgypal Z, Ariel F, Jegu T, Benhamed M, Szucs A, Kereszt A, Mergaert P, Kondorosi E. 2017. Ploidy-dependent changes in the epigenome of symbiotic cells correlate with specific patterns of gene expression. *Proceedings of the National Academy of Sciences, USA* **114**: 4543–4548.

Nallu S, Silverstein KAT, Samac DA, Bucciarelli B, Vance CP, VandenBosch KA. 2013. Regulatory patterns of a large family of defensin-like genes expressed in nodules of *Medicago truncatula*. *PLoS ONE* **8**: e60355.

Oldroyd GED, Downie JA. 2008. Coordinating nodule morphogenesis with rhizobial infection in legumes. *Annual Review of Plant Biology* **59**: 519–546.

Oono R, Denison RF. 2010. Comparing symbiotic efficiency between swollen versus nonswollen rhizobial bacteroids. *Plant Physiology* **154**: 1541–1548.

Ovchinnikova E, Journet EP, Chabaud M, Cosson V, Ratet P, Duc G, Fedorova E, Liu W, den Camp RO, Zhukov V *et al.* 2011. IPD3 controls the formation of nitrogen-fixing symbiosomes in pea and *Medicago* spp. *Molecular Plant–Microbe Interactions* **24**: 1333–1344.

Pan HR, Wang D. 2017. Nodule cysteine-rich peptides maintain a working balance during nitrogen-fixing symbiosis. *Nature Plants* **3**: 17048.

Ribeiro CW, Baldacci-Cresp F, Pierre O, Larousse M, Benyamina S, Lambert A, Hopkins J, Castella C, Cazareth J, Alloing G *et al.* 2017. Regulation of differentiation of nitrogen-fixing bacteria by microsymbiont targeting of plant thioredoxin s1. *Current Biology* **27**: 250–256.

Roux B, Rodde N, Jardinaud MF, Timmers T, Sauviac L, Cottret L, Carrere S, Sallet E, Courcelle E, Moreau S *et al.* 2014. An integrated analysis of plant and bacterial gene expression in symbiotic root nodules using laser-capture microdissection coupled to RNA sequencing. *The Plant Journal* **77**: 817–837.

Roy P, Achom M, Wilkinson H, Lagunas B, Gifford ML. 2020. Symbiotic outcome modified by the diversification from 7 to over 700 nodule-specific cysteine-rich peptides. *Genes* **11**: 348.

Sagan M, Morandi D, Tarenghi E, Duc G. 1995. Selection of nodulation and mycorrhizal mutants in the model plant *Medicago truncatula* (Gaertn) after gamma-ray mutagenesis. *Plant Science* **111**: 63–71.

Sankari S, Babu VMP, Bian K, Alhhazmi A, Andorfer MC, Avalos DM, Smith TA, Yoon K, Drennan CL, Yaffe MB *et al.* 2022. A haem-sequestering plant peptide promotes iron uptake in symbiotic bacteria. *Nature Microbiology* **7**: 1453–1465.

Starker CG, Parra-Colmenares AL, Smith L, Mitra RM, Long SR. 2006. Nitrogen fixation mutants of *Medicago truncatula* fail to support plant and bacterial symbiotic gene expression. *Plant Physiology* **140**: 671–680.

Terpolilli J, O'Hara G, Tiwari R, Dilworth M, Howieson J. 2008. The model legume *Medicago truncatula* A17 is poorly matched for N_2 fixation with the sequenced microsymbiont *Sinorhizobium meliloti* 1021. *New Phytologist* **179**: 62–66.

Van de Velde W, Guerra JCP, De Keyser A, De Rycke R, Rombauts S, Maunoury N, Mergaert P, Kondorosi E, Holsters M, Goormachtig S. 2006. Aging in legume symbiosis. A molecular view on nodule senescence in *Medicago Truncatula*. *Plant Physiology* **141**: 711–720.

Van de Velde W, Zehirov G, Szatmari A, Debreczeny M, Ishihara H, Kevei Z, Farkas A, Mikulass K, Nagy A, Tiricz H *et al.* 2010. Plant peptides govern terminal differentiation of bacteria in symbiosis. *Science* **327**: 1122–1126.

Vasse J, de Billy F, Camut S, Truchet G. 1990. Correlation between ultrastructural differentiation of bacteroids and nitrogen fixation in alfalfa nodules. *Journal of Bacteriology* **172**: 4295–4306.

Velivelli SLS, Czymmek KJ, Li H, Shaw JB, Buchko GW, Shah DM. 2020. Antifungal symbiotic peptide NCR044 exhibits unique structure and multifaceted mechanisms of action that confer plant protection. *Proceedings of the National Academy of Sciences, USA* **117**: 16043–16054.

Wang C, Yu HX, Luo L, Duan LJ, Cai LY, He XX, Wen JQ, Mysore KS, Li GL, Xiao AF *et al.* 2016. *NODULES WITH ACTIVATED DEFENSE 1* is required for maintenance of rhizobial endosymbiosis in *Medicago truncatula*. *New Phytologist* **212**: 176–191.

Wang D, Griffitts J, Starker C, Fedorova E, Limpens E, Ivanov S, Bisseling T, Long S. 2010. A nodule-specific protein secretory pathway required for nitrogen-fixing symbiosis. *Science* **327**: 1126–1129.

Wang Q, Yang SM, Liu JG, Terecskei K, Abraham E, Gombar A, Domonkos A, Szucs A, Kormoczi P, Wang T *et al.* 2017. Host-secreted antimicrobial peptide enforces symbiotic selectivity in *Medicago truncatula*. *Proceedings of the National Academy of Sciences, USA* **114**: 6854–6859.

Wei F, Liu Y, Zhou DL, Zhao WL, Chen ZN, Chen DS, Li YG, Zhang XX. 2022. Transcriptomic identification of a unique set of nodule-specific cysteine-rich peptides expressed in the nitrogen-fixing root nodule of *Astragalus sinicus*. *Molecular Plant–Microbe Interactions* **35**: 893–905.

Xi JJ, Chen YH, Nakashima J, Wang SM, Chen RJ. 2013. *Medicago truncatula esn1* defines a genetic locus involved in nodule senescence and symbiotic nitrogen fixation. *Molecular Plant–Microbe Interactions* **26**: 893–902.

Yang SM, Wang Q, Fedorova E, Liu JG, Qin QL, Zheng QL, Price PA, Pan HR, Wang D, Griffitts JS *et al.* 2017. Microsymbiont discrimination mediated by a host-secreted peptide in *Medicago truncatula*. *Proceedings of the National Academy of Sciences, USA* **114**: 6848–6853.

Zorin EA, Kliukova MS, Afonin AM, Gribchenko ES, Gordon ML, Sulima AS, Zhernakov AI, Kulaeva OA, Romanyuk DA, Kusakin PG *et al.* 2022. A variable gene family encoding nodule-specific cysteine-rich peptides in pea (*Pisum sativum* L.). *Frontiers in Plant Science* **13**: 884726.

Supporting Information

Additional Supporting Information may be found online in the Supporting Information section at the end of the article.

Fig. S1 Strain dependence of the symbiotic phenotype of mutants *Mtdnf7-2*, *Mtdnf4-1*, NF-FN9363 and *Mtsym20*.

Fig. S2 Transcriptional activity of senescence and defence-related marker genes in the nodules of symbiotic mutants NF-FN9363, *Mtsym20*, *Mtdnf4-1*, *Mtdnf7-2* and *nad1-3*.

Fig. S3 Scanning electron microscopy analysis of symbiotic cells and bacteroid morphology in NF-FN9363, *Mtsym20*, *Mtdnf7-2*, *Mtdnf4-1* mutant and wild-type nodules.

Fig. S4 Chromosomal position of the symbiotic loci of mutants NF-FN9363, *Mtsym19* and *Mtsym20* and the allelism test between *Mtsym19* and *Mtsym20*.

Fig. S5 Estimating the size of the deletion in the symbiotic locus of NF-FN9363.

Fig. S6 Complementation of NF-FN9363, *Mtsym20* and *Mtsym19* symbiotic mutants.

Fig. S7 Estimating the size of the deletion in the symbiotic loci of *Mtsym20* and *Mtsym19*.

Methods S1 Supplementary details to Materials and Methods.

Table S1 Primers used in this study.

Please note: Wiley is not responsible for the content or functionality of any Supporting Information supplied by the authors. Any queries (other than missing material) should be directed to the *New Phytologist* Central Office.